Fractal-Based Point Processes

2005

Steven Bradley Lowen

Harvard Medical School
McLean Hospital

Malvin Carl Teich

Boston University
Columbia University

WILEY

6

Processes Based on Fractional Brownian Motion

The Russian mathematician **Andrei Nikolaevich Kolmogorov (1903–1987)** substantially advanced the art of stochastic processes, particularly those involving turbulence and scaling; he formulated the concept of fractional Brownian motion in 1940.

Together with Benoit Mandelbrot, the American probabilist **John W. Van Ness (born 1936)** carried out a seminal study in 1968 that used the concept of self-similarity to advance the theory of fractional Brownian motion.

This chapter sets forth the properties of fractional Brownian motion, fractional Gaussian noise, and several related fractal processes. These continuous-time processes serve handily as rates for point processes. When used as the drivers for doubly stochastic or integrate-and-reset constructs, they impart their fractal characteristics to the ensuing fractal-rate point processes, thereby providing useful models for a variety of phenomena. Moreover, under suitable circumstances a number of non-Gaussian fractal-rate processes converge to these Gaussian processes. An excellent overview of the properties of fractional Brownian motion (Sec. 6.1) and fractional Gaussian noise (Sec. 6.2) has recently been provided by Taqqu (2003).

6.1 FRACTIONAL BROWNIAN MOTION

A concise mathematical description of ordinary Brownian motion (as represented by the Wiener–Lévy process) was provided in Sec. 2.4.2. The elements of **fractional Brownian motion**, an important generalization, were set forth by Kolmogorov (1940) and extensively developed by Mandelbrot & Van Ness (1968). A brief historical account of fractional Brownian motion has recently been provided by Molchan (2003).

6.1.1   Definition

Fractional Brownian motion, $B_H(t)$, is defined using the same three features that we specified for ordinary Brownian motion, $B(t)$: the amplitude distribution, the mean, and the autocorrelation. Like ordinary Brownian motion, fractional Brownian motion is Gaussian (Mandelbrot & Van Ness, 1968): a vector $\{B_H(t_1), B_H(t_2), ..., B_H(t_k)\}$, for any positive integer k and any set of times $\{t_1, t_2, ..., t_k\}$, has a joint Gaussian distribution. Fractional Brownian motion, as usually defined, also belongs to the zero-mean class of stochastic processes: $\mathrm{E}[B_H(t)] = 0$ for all t.

The distinction between the fractional and ordinary versions thus lies in their autocorrelations. For fractional Brownian motion the autocorrelation takes the form (Kolmogorov, 1940; Mandelbrot & Van Ness, 1968)

$$\mathrm{E}[B_H(s)\,B_H(t)] = \tfrac{1}{2}\mathrm{E}[B_H^2(1)]\left(|t|^{2H} + |s|^{2H} - |t-s|^{2H}\right), \qquad (6.1)$$

with (Barton & Poor, 1988)

$$\mathrm{E}[B_H^2(1)] = \Gamma(1-2H)\,\cos(\pi H)/(\pi H). \qquad (6.2)$$

The parameter H, known as the **Hurst exponent**, assumes values between zero and unity. For $H = \tfrac{1}{2}$, $B_H(t)$ is ordinary Brownian motion so that $B_{\frac{1}{2}}(t) \equiv B(t)$ (Mandelbrot & Van Ness, 1968). Hurst's (1951; 1956; 1965) pioneering work on long-range correlations in river flows, for which he developed rescaled range analysis as described in Sec. 3.3.5, also served as a precursor to fractional Brownian motion and its related processes (Mandelbrot, 1965b, 1982).

Fractional Brownian motion can be expressed in terms of ordinary Brownian motion:

$$\begin{aligned}
\Gamma(H+\tfrac{1}{2})\,B_H(t) &= \int_{-\infty}^{0}\left[(t-s)^{H-1/2} - (-s)^{H-1/2}\right]dB(s) \\
&\quad + \int_{0}^{t}(t-s)^{H-1/2}\,dB(s) \qquad (6.3) \\
&= \int_{-\infty}^{t}(t-s)^{H-1/2}\,dB(s) \\
&\quad - \int_{-\infty}^{0}(-s)^{H-1/2}\,dB(s). \qquad (6.4)
\end{aligned}$$

Indeed, this relationship often serves as a definition of fractional Brownian motion (Mandelbrot & Van Ness, 1968). Equation (6.3) comprises convergent integrals, whereas Eq. (6.4) exhibits more symmetry at the expense of employing divergent integrals (although with the same, convergent difference).

The standard deviation of fractional Brownian motion varies as t^H, so that this process is not stationary. However, manipulation of Eqs. (6.1), (6.3), or (6.4) reveals that fractional Brownian motion does have stationary increments:

$$\Pr\{B_H(t_2+s) - B_H(t_2) > x\} = \Pr\{B_H(t_1+s) - B_H(t_1) > x\} \qquad (6.5)$$

for all times s, t_1, t_2, and for all amplitudes x.

6.1.2 Properties

Like ordinary Brownian motion, fractional Brownian motion contains statistical copies of itself (Mandelbrot & Van Ness, 1968). Scaling the time axis of Eq. (6.1) by a factor a yields a new process $B_H(at)$ with autocorrelation

$$\mathrm{E}[B_H(as)\,B_H(at)] = |a|^{2H}\,\mathrm{E}[B_H(s)\,B_H(t)]; \qquad (6.6)$$

scaling the amplitude directly by b yields $bB_H(t)$, with autocorrelation

$$\mathrm{E}[bB_H(s)\,bB_H(t)] = b^2\,\mathrm{E}[B_H(s)\,B_H(t)]. \qquad (6.7)$$

By construction, both $B_H(at)$ and $bB_H(t)$ also have zero mean and belong to the Gaussian family of processes. Setting $|b| \equiv |a|^H$ makes the two autocorrelations coincide, and since the mean and autocorrelation uniquely determine a Gaussian process (Feller, 1971), $B_H(at)$ and $|a|^H B_H(t)$ are statistically identical. Thus, changing the time axis by a scale a and the amplitude axis by a scale $|a|^H$ yield the same result, and $B_H(t)$ contains statistical copies of itself at any scale. This argument generalizes the result set forth at the end of Sec. 2.4.2.

The definition provided in Sec. 6.1.1 leads to a number of other properties, including level-crossing statistics and generalizations of the spectrum. Level crossings of fractional Brownian motion, like those of ordinary Brownian motion, yield a degenerate point process; in any neighborhood about any level crossing, an infinite number of other crossings exist. The same degeneracy occurred for the Lévy dust encountered in Sec. 4.7, which this set of level crossings closely resembles. Imposing a minimum resolvable interevent time A results in a well-defined point process, for which the interevent-interval density $p_\tau(t)$ follows the Pareto form (Ding & Yang, 1995)

$$p_\tau(t) = (1 - H)\,A^{1-H}\,t^{H-2}, \quad t > A. \qquad (6.8)$$

For $H \neq \frac{1}{2}$, this point process exhibits dependencies among the interevent intervals, and therefore does not belong to the renewal family of point processes.

As a result of its nonstationarity, difficulties arise in calculating the spectrum of fractional Brownian motion. The Wigner–Ville spectrum (Ville, 1948), $S_{W,X}(t, f)$, a generalization of the conventional spectrum, provides one solution to this problem. For a continuous-time real-valued process $X(t)$, this generalized spectrum takes the form

$$S_{W,X}(t, f) = \int_{-\infty}^{\infty} \left\{ \mathrm{E}[X(t + s/2)\,X(t - s/2)] - \mathrm{E}^2[X] \right\} e^{-i2\pi f s}\, ds. \qquad (6.9)$$

For a wide-sense stationary process, the Wigner–Ville spectrum reduces to the conventional spectrum: $S_{W,X}(t, f) = S_X(f)$ for all t.

Applied to fractional Brownian motion, this transform yields (Flandrin, 1989)

$$S_{W,B_H}(t, f) = \left[1 - 2^{1-2H} \cos(4\pi f t) \right] |2\pi f|^{-(2H+1)}. \qquad (6.10)$$

In a number of publications, the factor standing to the right of the brackets in Eq. (6.10) is presented out of context, as if it had arisen from a conventional spectrum. This

has led to the (false) impression that fractional Brownian motion has a true spectrum that decays as $f^{-(2H+1)}$. Since this process is nonstationary, it does not possess a conventional spectrum.

6.1.3 Synthesis

A variety of synthesis techniques exist for generating discrete-time samples of fractional Brownian motion. An excellent overview of simulation methods, including their accuracies and efficiencies, has been provided by Bardet, Lang, Oppenheim, Philippe & Taqqu (2003). An early exact, but slow [$O(M^3)$], method employed Cholesky decomposition of the complete autocorrelation matrix (Lundahl, Ohley, Kay & Siffert, 1986). Subsequent approximate methods reduced computational load [$O(M \log M)$] at the expense of exact results; these include spectral and midpoint displacement methods (Peitgen & Saupe, 1988), improved spectral methods (Timmer & König, 1995), and wavelet approaches (Tewfik & Kim, 1992; Flandrin, 1992; Stoksik, Lane & Nguyen, 1994; Sellan, 1995; Abry & Sellan, 1996).

For $0 < H \leq \frac{1}{2}$ only, an exact and fast [$O(M \log M)$] method is available (Lowen, 2000). It begins with a periodic discrete-time autocorrelation $R_x(n)$ proportional to $1 - |n/M|^{2H}$ for $|n| \leq M$. Succeeding steps involve transforming this function into the Fourier domain, taking the square root, randomizing the phase and amplitude, transforming back, and subtracting the first element of the resulting sequence from the rest. This final series yields M exact samples of fractional Brownian motion, with a computational load of order $M \log(M)$. Another efficient exact method relies on circulant matrices and enjoys fast computation time [$O(M \log M)$], although minimum values for M exist (Davies & Harte, 1987).

6.1.4 Realizations

Figure 6.1 displays fractional Brownian motion for five different values of H (0.1, 0.3, 0.5, 0.7, and 0.9). The realization for $H = 0.5$ corresponds to ordinary Brownian motion (see also Fig. 2.2). To highlight the differences engendered by changing the value of H, we employ the same underlying white Gaussian random variables for generating all curves.

For convenience, we employ the improved spectral method, retaining 500 samples from a Fourier transform of length $2^{19} = 524288$, or just under 0.1%. A fraction as small as this results in negligible error. We normalize the plots so that all have a range of unity, from minimum to maximum displayed values, and we displace them from each other by unity.

Although the same statistical fluctuations appear in all five simulations, increasing the fractional-Brownian-motion parameter H leads to smoother curves. Qualitatively, larger values of H have generalized spectra that decay more quickly with frequency [see Eq. (6.10)]. Accordingly, these curves display a greater proportion of fluctuations at larger time scales than those for smaller values of H, and therefore appear smoother.
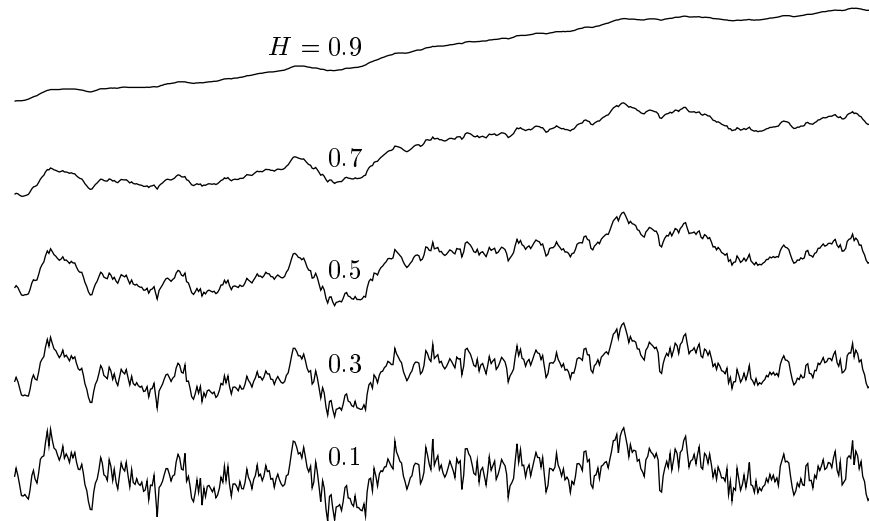
Fig. 6.1 Realizations of fractional Brownian motion for $H = 0.1, 0.3, 0.5, 0.7$, and 0.9, with H largest at the top. Corresponding values of the fractal exponent are $\alpha = 2H + 1 = 1.2$, 1.6, 2.0, 2.4, and 2.8, respectively (the relationship between H and α is provided in Sec. 6.3). The same random seed serves for all five curves, so that they all have similar features. Larger values of H and α yield smoother curves.

Generalized dimensions provide a precise description of this smoothness, and for true fractional Brownian motion (not the discrete-time approximations displayed in Fig 6.1), the various generalized dimensions yield a value of $2 - H$ for the motion itself, and $1 - H$ for its level crossings (Mandelbrot, 1982). Smaller values of H yield larger generalized dimensions, consistent with rougher curves. As H approaches unity, the generalized dimensions of fractional Brownian motion also approach unity, the value for a nonfractal, perfectly smooth curve.

6.1.5 Rate process

In serving as a rate for a point process, fractional Brownian motion exhibits two difficulties: nonstationarity and negative values. One solution to the nonstationarity issue involves imparting a cutoff at low frequencies, effectively imposing a longest time scale. An approximation of this kind yields useful results in many cases and can greatly simplify the associated theoretical and computational tasks. Other techniques are also available, including nonlinear ones such as resetting the fractional Brownian motion when it reaches a certain threshold, but these lead to more significant deviations from ideal behavior and to increased mathematical complexity.

Negative values, which do not make sense for a point-process rate, can be handled by offset, nonlinear transform, or both. The offset method, applied to a process ren-

dered stationary by including a low-frequency cutoff, makes use of a mean value that is significantly larger than the standard deviation, so that the resulting fractional Brownian motion essentially always remains positive. The nonlinear transform method uses a nonlinear function $f(x)$ that generates a nonnegative output regardless of the input x, but this is achieved at the price of distorting the process. Candidate functions include $f(x) = (x + |x|)/2$, as well as smoother and more complex forms such as $f(x) = c \ln(1 + e^{x/c})$ for some constant $c > 0$.

6.2 FRACTIONAL GAUSSIAN NOISE

Fractional Gaussian noise $B'_H(t)$ represents the derivative of fractional Brownian motion, much as white Gaussian noise represents the derivative of ordinary Brownian motion.

6.2.1 Definition

Like white Gaussian noise, **fractional Gaussian noise** does not exist in a mathematical sense since fractional Brownian motion does not have a proper derivative. In contrast to fractional Brownian motion, where introducing a low-frequency cutoff ameliorates the effects of nonstationarity, a tractable approximation for fractional Gaussian noise is attained by introducing a high-frequency cutoff.

Perhaps the simplest method for obtaining fractional Gaussian noise in the face of the nondifferentiability of fractional Brownian motion entails convolving the latter with a rectangular filter before forming the derivative (Mandelbrot & Van Ness, 1968):

$$
\begin{aligned}
B'_{H2}(t,v) &= v^{-1} \frac{d}{dt} \int_{t-v/2}^{t+v/2} B_H(u)\, du \\
&= \frac{B_H(t + v/2) - B_H(t - v/2)}{v}.
\end{aligned} \tag{6.11}
$$

This yields a process whose statistics resemble those of true fractional Gaussian noise, for time scales significantly greater than the separation time v. Other piecewise smooth filter functions yield similar results, but with increased mathematical complexity.

6.2.2 Properties

Combining Eqs. (6.9), (6.10), and (6.11) provides the Wigner–Ville spectrum of this filtered version of fractional Gaussian noise,

$$
S_{W,B'_{H2}}(t,v,f) = 4v^{-2} |2\pi f|^{-(2H+1)} \sin^2(\pi f v) \tag{6.12}
$$

$$
\lim_{v \to 0} S_{W,B'_{H2}}(t,v,f) = |2\pi f|^{-(2H-1)}, \tag{6.13}
$$

where Eq. (6.13) yields the same result as that obtained for true fractional Gaussian noise $B'_H(t)$ using direct methods (Flandrin, 1989). Thus, true fractional Gaussian

noise has a spectrum that follows a pure power-law decaying form, as does its approximation $B'_{H2}(t, v)$ for frequencies much lower than the effective cutoff frequency $f_S = (2\pi v)^{-1}$. Neither Eq. (6.12) nor Eq. (6.13) depend on time since both fractional Gaussian noise and its filtered version are stationary. Equation (6.12) does depend on v, but this is a filter parameter.

6.2.3   Synthesis

As a stationary process, fractional Gaussian noise has an autocorrelation with only one argument. Since the process also has a zero mean, this single-argument function completely specifies the fractional Gaussian noise process, simplifying simulation considerably.

A simpler variant of the method delineated by Lowen (2000) generates discrete-time realizations of fractional Gaussian noise for $H > \frac{1}{2}$ only (Davies & Harte, 1987). However, running sums of this process do not yield realizations of fractional Brownian motion; generating the latter over an interval $(0, t)$ from fractional Gaussian noise requires integrating over all times within that interval. Samples of fractional Gaussian noise lack information about the process at times other than the samples, and therefore cannot generate a proper integral of the underlying continuous-time fractional Gaussian noise. Similarly, differencing discrete-time samples of fractional Brownian motion does not yield samples of fractional Gaussian noise.

6.2.4   Realizations

Figure 6.2 displays fractional Gaussian noise for four different values of H (0.1, 0.3, 0.7, and 0.9), as well as for white Gaussian noise ($H = 0.5$) (see also Mandelbrot & Wallis, 1969a). To highlight the differences associated with various values of H, we again employ the same underlying white Gaussian random variables to generate all curves. Simulation methods, including the underlying random variables, follow those used for producing Fig. 6.1.

Again, increasing H leads to smoother curves, albeit with similar statistical fluctuations. In contrast to the results for fractional Brownian motion displayed in Fig. 6.1, these curves fill part of the plane near their mean values, so that the generalized dimensions assume a value of two in all cases. Similarly, the level crossing sets all have generalized dimensions of unity.

6.2.5   Rate process

Unlike fractional Brownian motion, fractional Gaussian noise is stationary. Like fractional Brownian motion, however, it can assume negative values. To enable fractional Gaussian noise to serve as a rate, the same methods used to ameliorate the negative-value shortcoming of fractional Brownian motion can be used for fractional Gaussian noise as well (see Sec. 6.1.5).
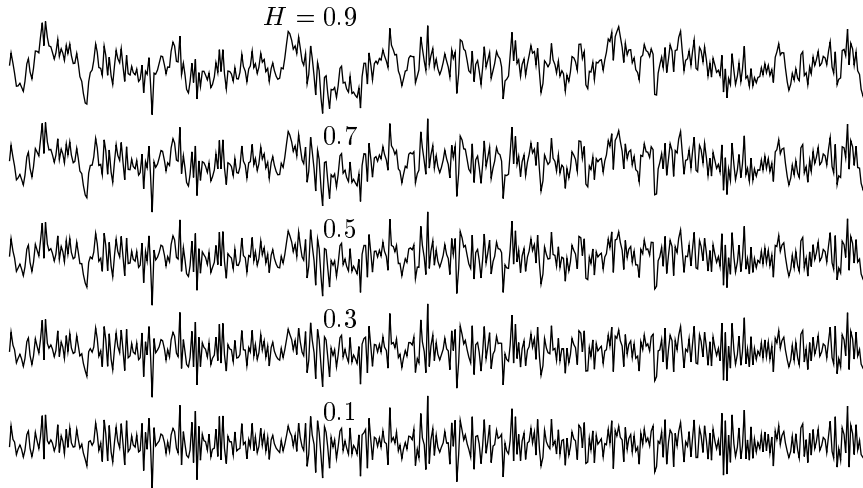
Fig. 6.2 Realizations of fractional Gaussian noise for $H = 0.1, 0.3, 0.5, 0.7,$ and 0.9, with H largest at the top. Corresponding values of the fractal exponent are $\alpha = 2H - 1 = -0.8, -0.4, 0.0, 0.4,$ and 0.8, respectively (the relationship between H and α appears in Sec. 6.3). The same random seed serves for all five curves (as well as for the five curves in Fig. 6.1) so that all have similar features. The curves become somewhat smoother as H and α increase.

6.3 NOMENCLATURE FOR FRACTIONAL PROCESSES

6.3.1 Relationship between Hurst and scaling exponents

Fractional Brownian motion and fractional Gaussian noise have heretofore been defined in terms of the Hurst exponent H. Since most other processes are cast in terms of the scaling exponent α, we proceed to relate these two parameters.

We have thus far defined H in accordance with common usage: it lies between zero and unity for *both* fractional Brownian motion and fractional Gaussian noise (Mandelbrot & Van Ness, 1968; Barton & Poor, 1988). We know, however, that the spectrum of fractional Gaussian noise (FGN) varies as $f^{-\alpha} = f^{-(2H-1)}$ whereas that for a stationary version of fractional Brownian motion (FBM) varies as $f^{-\alpha} = f^{-(2H+1)}$. Thus, different relations are required to connect the exponents, depending on the process:

$$
\begin{array}{llll}
\text{FGN:} & \alpha = 2H - 1 & & -1 < \alpha < 1 \\
\text{FBM:} & \alpha = 2H + 1 & 0 < H < 1 & 1 < \alpha < 3.
\end{array}
\tag{6.14}
$$

However, the relationship between H and α applicable for fractional Brownian motion is sometimes also taken to apply to fractional Gaussian noise (Mandelbrot, 1982;

Flandrin, 1992). This requires that H span different ranges for the two processes:

$$\begin{array}{llll} \text{FGN:} & & -1 < H < 0 & -1 < \alpha < 1 \\ \text{FBM:} & \alpha = 2H + 1 & 0 < H < 1 & 1 < \alpha < 3. \end{array} \qquad (6.15)$$

Since the ranges of H differ in Eqs. (6.14) and (6.15), whereas those for α remain the same, using the latter exponent avoids confusion. Hence, we generally eschew the Hurst exponent H in favor of the scaling exponent α. We do continue to refer to fractional Brownian motion as $B_H(t)$, however.

6.3.2 Fractional integration

It is clear from Eqs. (6.14) and (6.15) that the ranges of the exponent α for fractional Gaussian noise and fractional Brownian motion differ by the integer two. This results from a simple property of integration: the power-law exponent of the spectrum increases by precisely two (differentiation results in a decrease of the exponent by precisely two). More generally, the n-fold integration of a process results in an increase in the exponent by $2n$.

Generalizing still further, x-fold Riemann–Liouville fractional integration corresponds to an increase in the exponent by $2x$ (see, for example, Pipiras & Taqqu, 2003). Such fractional integration provides a method for generating fractional Brownian motion and fractional Gaussian noise from white Gaussian noise (Barnes & Allan, 1966; Mandelbrot, 1967b; Maccone, 1981). Equations (6.3) and (6.4) represent just such an operation, with the kernels in these integrals representing fractional integration of degree $\alpha/2$ operating on the ordinary Brownian motion process $B(t)$ (Mandelbrot & Van Ness, 1968; Pipiras & Taqqu, 2003).

6.3.3 Fractal Gaussian processes

We do not intend to imply that fractional Brownian motion and fractional Gaussian noise behave identically; they certainly differ in their stationarity. However, since we focus on stationary processes throughout this book, we impose cutoffs on these two processes when necessary, thereby obviating any differences associated with the issue of stationarity.

Another distinction lies in some measures that provide useful scaling results for fractional Gaussian noise, but not for fractional Brownian motion; this is a result of the different ranges spanned by α in the two cases. For this reason, some authors have suggested employing different methods for analyzing fractional Brownian motion and fractional Gaussian noise (Raymond & Bassingthwaighte, 1999). However, if we bear in mind the limited ranges of the various measures set forth in Sec. 5.2 and, in particular, if we choose measures that prove useful for both processes, the significance of this difference is reduced.

With the differences between fractional Brownian motion and fractional Gaussian noise diminished in this context, it proves simpler and more accurate to refer to this family of processes as **fractal Gaussian processes**, indexed by a spectral power-law exponent α that may take any positive value (we specifically exclude fractional

Gaussian noise with $\alpha \leq 0$ from this class for the reasons set forth in Sec. 5.2.1). We then consider Figs. 6.2 and 6.1 as a unit; they display fractal Gaussian processes with increasing smoothness as the value of α climbs from $0+$ to 2.8.

With negative values of α eliminated, and low-frequency cutoffs for $\alpha \geq 1$ imposed, the family of fractal Gaussian processes can dutifully serve as rate processes, thereby enabling the construction of doubly stochastic Poisson point processes (Sec. 4.3) and integrate-and-reset point processes (Sec. 4.4). Indeed, the integration inherent in both of these constructions smoothes the rate sufficiently to render high-frequency cutoffs unnecessary. Gaussian processes are convenient as rates because they are ubiquitous and are fully characterized by their means and covariances; this facilitates comparison with experiment. Moreover, they emerge from fractal binomial noise and fractal shot noise in important limits, as discussed in Secs. 8.3.2 and 10.6.1, respectively.

This process has, in fact, been used as a rate for a doubly stochastic Poisson process, resulting in the **fractal-Gaussian-process-driven Poisson process** (see Fig. 5.5 as well as Secs. 8.4 and 10.6.1). Because of its widespread applicability, we have chosen it for the analysis and estimation studies carried out in Chapter 12.

In the domain of neurophysiology, for example, it is useful for modeling sequences of action potentials. In particular, it has served as a valuable point of departure for characterizing mammalian auditory-nerve action potentials for high-frequency stimuli (Teich, Turcott & Lowen, 1990; Teich, 1992; Lowen & Teich, 1993b). Low-frequency stimuli are accommodated by forming a driving function from the superposition of a fractal Gaussian process and the modulating stimulus. When modified to accommodate the effects of neural refractoriness (see Sec. 11.2.4), the dead-time-modified version of this process characterizes essentially all of the observable aspects of auditory neural spike trains elicited by a broad range of stimuli, over a broad range of time scales (Lowen & Teich, 1996b, 1997). We point out, however, that alternative fractal-based point-process constructs have also been formulated to describe the auditory neural spike train (see Secs. 6.4, 6.6, and 8.4).

In a similar manner, the **fractal-Gaussian-process-driven integrate-and-reset process** serves as an excellent model for action-potential generation in the peripheral visual system, provided that the rate process comprises a superposition of a fractal Gaussian process and the modulating stimulus, and that neural refractoriness (see Sec. 11.2.4) is accommodated (Teich & Lowen, 2003). Furthermore, imparting random displacement (see Sec. 11.3) to the fractal-Gaussian-process-driven integrate-and-reset process yields a model that serves as a good descriptor for the sequence of human heartbeats (Teich et al., 2001). Nonfractal point processes serve as suitable models only over short time scales.

6.4   FRACTAL CHI-SQUARED NOISE

The nonlinear transforms provided at the end of Sec. 6.1.5 ensure nonnegative rate functions while introducing a minimum of change in the Gaussian amplitude distribu-

tion. For some applications, however, amplitude distributions other than the Gaussian prove useful. As one example, we examine the properties of chi-squared noise.

If $\{X_k(t)\}$, $1 \leq k \leq M$, represents a collection of M independent and identically distributed Gaussian processes with zero mean, variance $\mathrm{Var}[X]$, and autocorrelation $R_X(t)$, then $\mu(t) \equiv \sum_{k=1}^{M} X_k^2(t)$ has an autocorrelation given by

$$
\begin{aligned}
R_\mu(t) &\equiv \mathrm{E}\left[\sum_{n=1}^{M} X_n^2(s) \sum_{m=1}^{M} X_m^2(s+t)\right] = \sum_{n=1}^{M} \sum_{m=1}^{M} \mathrm{E}\left[X_n^2(s)\, X_m^2(s+t)\right] \\
&= \sum_{n=1}^{M} \left(\mathrm{E}\left[X_n^2(s)\, X_n^2(s+t)\right] + \sum_{m \neq n} \mathrm{E}\left[X_n^2(s)\, X_m^2(s+t)\right]\right) \\
&= \sum_{n=1}^{M} \left(2R_X^2(t) + \mathrm{E}[X^2]\,\mathrm{E}[X^2] + \sum_{m \neq n} \mathrm{E}[X^2]\,\mathrm{E}[X^2]\right) \\
&= 2MR_X^2(t) + \mathrm{E}^2[\mu].
\end{aligned}
\tag{6.16}
$$

In deriving this result, we have made use of the independence of the component fractal Gaussian processes $X_k(t)$ that comprise $\mu(t)$, along with the well-known property

$$
\begin{aligned}
\mathrm{E}[X_1 X_2 X_3 X_4] &= \mathrm{E}[X_1 X_2]\,\mathrm{E}[X_3 X_4] \\
&+ \mathrm{E}[X_1 X_3]\,\mathrm{E}[X_2 X_4] \\
&+ \mathrm{E}[X_1 X_4]\,\mathrm{E}[X_2 X_3]
\end{aligned}
\tag{6.17}
$$

for any four zero-mean jointly Gaussian random variables $\{X_1, X_2, X_3, X_4\}$.

The process $\mu(t)$ then has a chi-squared (χ^2) distribution with M degrees of freedom (Feller, 1971). Standard probability theory yields the statistics of this amplitude, including the probability density function

$$
p_\mu(y) = [\Gamma(M/2)]^{-1} \left(2\mathrm{Var}[X]\right)^{-M/2} y^{M/2-1} \exp\left(-y/2\mathrm{Var}[X]\right)
\tag{6.18}
$$

and moments

$$
\mathrm{E}[\mu^n] = \frac{\Gamma(n+M/2)}{\Gamma(M/2)} \left(2\mathrm{Var}[X]\right)^n.
\tag{6.19}
$$

If $X(t)$ belongs to the fractal class of continuous processes, with fractal exponent α_X in the range $\frac{1}{2} < \alpha_X < 1$, then $R_\mu(t)$ also exhibits scaling, but with the exponent $\alpha_\mu = 2\alpha_X - 1$ (Thurner et al., 1997, see also Prob. 6.6). The result is **fractal chi-squared noise**. Setting $M = 2$ yields **fractal exponential noise** since the χ^2 distribution with two degrees of freedom is the exponential distribution.

The chi-squared distribution with $2M$ degrees of freedom successfully models a whole host of phenomena, including the energy fluctuations of multimode thermal light (Mandel, 1959; Saleh, 1978) and multimode acoustic noise (McGill, 1967). Smearing the mean of a Poisson counting kernel with the chi-squared distribution yields the associated photon-counting and neural-counting distributions for these two processes. The result is the **negative binomial counting distribution** (Mandel, 1959;

McGill, 1967), the origin of which resides in Greenwood & Yule's (1920) seminal study of accident occurrences.

A related model employs the sum of the squares of positive-mean Gaussian noise processes, which generates noncentral chi-squared noise. If the components belong to the fractal class of continuous processes, the outcome is **fractal noncentral chi-squared noise**. The presence of the nonzero mean modifies the second-order characteristics of the process so that, in some cases, two power-law regions emerge with both fractal exponents, α_X and α_μ, appearing in different ranges of the associated spectrum (see Prob. 6.6). Setting $M = 2$ yields **fractal noncentral Rician-squared noise**, since the noncentral chi-squared distribution with two degrees of freedom is the noncentral Rician-squared distribution (Rice, 1944, 1945; Saleh, 1978).[1]

Fractal noncentral chi-squared noise has also been used as a rate for a doubly stochastic Poisson point process, again to model mammalian auditory-nerve action potentials (Kumar & Johnson, 1993). The Poisson transform of the noncentral chi-squared distribution, which is known as the **noncentral negative binomial distribution**, has found extensive use in photon counting and neural counting (Peřina, 1967; McGill, 1967; Teich & McGill, 1976; Li & Teich, 1993).

6.5 FRACTAL LOGNORMAL NOISE

We consider an additional example of continuous rate process with a non-Gaussian amplitude that finds use in many contexts: **fractal lognormal noise**. The term "lognormal" refers to a random quantity whose logarithm follows a Gaussian (normal) form (Aitchison & Brown, 1957; Gumbel, 1958). The exponential transform of a fractal Gaussian process follows this form precisely and, furthermore, renders the resulting process strictly positive so that it may serve as a rate without further transformation.

Specifically, let $X(t)$ represent a Gaussian process with mean $\mathrm{E}[X]$, variance $\mathrm{Var}[X]$, and autocorrelation $R_X(t)$, and define a rate $\mu(t) \equiv \exp[X(t)]$. This rate then has the lognormal probability density function

$$p_\mu(y) = \left(2\pi \mathrm{Var}[X]\right)^{-1/2} y^{-1} \exp\left(-\left\{\ln(y) - \mathrm{E}[X]\right\}^2 / 2\mathrm{Var}[X]\right). \quad (6.20)$$

Straightforward application of probability theory yields the moments of the rate (see Lowen et al., 1997b, and Sec. A.3.1):

$$
\begin{aligned}
\mathrm{E}[\mu^n] &= \exp\left(n\,\mathrm{E}[X] + n^2\,\mathrm{Var}[X]/2\right) \\
\mathrm{E}[\mu] &= \exp\left(\mathrm{E}[X] + \mathrm{Var}[X]/2\right) \\
\mathrm{Var}[\mu] &= \exp\left(2\mathrm{E}[X]\right)\Big[\exp\left(2\mathrm{Var}[X]\right) - \exp\left(\mathrm{Var}[X]\right)\Big].
\end{aligned}
\quad (6.21)
$$

---

[1] A photograph of Rice stands at the beginning of Chapter 9.

After a fair amount of calculation, a result for the autocorrelation emerges (see Lowen et al., 1997b, and Sec. A.3.1):

$$R_\mu(t) = \mathrm{E}^2[\mu] \, \exp\{R_X(t) - \mathrm{E}^2[X]\}. \tag{6.22}$$

We point out that the exponential transform can lead to rather skewed distributions for μ. Substituting Eq. (6.21) into Eq. (3.4) yields a skewness given by

$$\mathrm{E}[(\mu - \mathrm{E}[\mu])^3]/\mathrm{Var}^{3/2}[\mu] = \left[\exp(\mathrm{Var}[X]) - 1\right]^{1/2} \left[\exp(\mathrm{Var}[X]) + 2\right]; \tag{6.23}$$

this quantity assumes large values for relatively small values of $\mathrm{Var}[X]$. As an example, $\mathrm{Var}[X] = 5$ yields a skewness of 1826. In contrast, an exponential distribution has a skewness of two, whereas a Gaussian has zero skewness.

With many of the properties of the rate $\mu(t)$ determined, we now consider point processes generated from this rate. We begin with the Poisson-process version. If we assume that the rate $\mu(t)$ exhibits fluctuations over frequency ranges significantly lower than the mean rate $\mathrm{E}[\mu]$, then closed-form expressions for the moments of the intervals τ between events exist (Lowen et al., 1997a,b):

$$\begin{aligned}
\mathrm{E}[\tau^n] &= n! \, \exp\left\{-n\,\mathrm{E}[X] + (n^2 - 2n)\,\mathrm{Var}[X]/2\right\} \\
\mathrm{E}[\tau] &= \exp\left(-\mathrm{E}[X] - \mathrm{Var}[X]/2\right) \\
\mathrm{Var}[\tau] &= \exp\left(-2\mathrm{E}[X]\right)\left[2 - \exp\left(-\mathrm{Var}[X]\right)\right],
\end{aligned} \tag{6.24}$$

where we have made use of Eq. (4.31). Employing Eq. (4.32) leads to the associated interevent-interval probability density (Lowen et al., 1997a),

$$\begin{aligned}
p_\tau(t) &= \pi^{-1/2} \, \exp\left(\mathrm{E}[X] + \tfrac{3}{2}\,\mathrm{Var}[X]\right) \\
&\quad \times \int_{-\infty}^{\infty} \exp\left[-y^2 - t\,\exp\left(\mathrm{E}[X] + 2\mathrm{Var}[X] + \sqrt{2\mathrm{Var}[X]}\,y\right)\right] dy.
\end{aligned} \tag{6.25}$$

For the integrate-and-reset version, we again require that the rate process $\mu(t)$ not exhibit fluctuations over frequencies comparable to, or higher than, the mean rate $\mathrm{E}[\mu]$. Using Eq. (4.38) provides results similar to those presented in Eq. (6.24):

$$\begin{aligned}
\mathrm{E}[\tau^n] &= \exp\left\{-n\,\mathrm{E}[X] + (n^2 - 2n)\,\mathrm{Var}[X]/2\right\} \\
\mathrm{E}[\tau] &= \exp\left(-\mathrm{E}[X] - \mathrm{Var}[X]/2\right) \\
\mathrm{Var}[\tau] &= \exp\left(-2\mathrm{E}[X]\right)\left[1 - \exp\left(-\mathrm{Var}[X]\right)\right],
\end{aligned} \tag{6.26}$$

while combining Eqs. (4.37) and (6.20) yields

$$\begin{aligned}
p_\tau(t) &= \left(2\pi\mathrm{Var}[X]\right)^{-1/2} \exp\left(-\mathrm{E}[X] - \mathrm{Var}[X]/2\right) \\
&\quad \times \exp\left(-\left\{\ln(t) + \mathrm{E}[X]\right\}^2/2\mathrm{Var}[X]\right) t^{-2}.
\end{aligned} \tag{6.27}$$

We now turn to the specific case where $X(t)$ belongs to the family of fractal Gaussian processes. The exponential transformation in Eq. (6.22) renders nonlinear the relationship between the autocorrelation of the input process $X(t)$ and that of the rate $\mu(t)$; in particular $S_N(f)$, the spectrum of the generated point process $dN(t)$, does not follow an exact power-law decay as we assume for $S_X(f)$. This holds true both for the doubly stochastic Poisson and integrate-and-reset versions. However, when $\text{Var}[X]$ is relatively small in comparison with unity, the forms of the two spectra do not differ greatly. Conversely, one can construct a Gaussian process with an appropriate autocorrelation such that the resulting lognormal noise has precisely fractal characteristics. For example, $R_X(t) = c_1 + (\alpha - 1) \ln |t|$, for $0 < \alpha < 1$, over a large range of delay times t, yields $S_N(f) = c_2 f^{-\alpha}$ over a corresponding range of frequencies f.

The **fractal lognormal-noise-driven Poisson process** turns out to be a suitable model for describing vesicular exocytosis (see Lowen et al., 1997a,b, as well as Prob. 6.8).

6.6   POINT PROCESS FROM ORDINARY BROWNIAN MOTION

Davidsen & Schuster (2002) have recently drawn attention to a simple but plausible method for generating fractal-based point processes from ordinary Brownian motion (see also Kaulakys, 1999). Their construct resembles a conventional integrate-and-reset process but differs in that the threshold, rather than the integration rate, is taken to be a stochastic process.

This kind of behavior occurs in neurophysiology, for example, where ion-channel current fluctuations give rise to random threshold fluctuations. A variety of models have been used to introduce such "fluctuations in excitability" (Pecher, 1939; Verveen & Derksen, 1968; Holden, 1976, Chapters 1 and 4). In one well-established recipe, the threshold undergoes diffusion, with or without drift, resulting in interval statistics that obey the inverse-Gaussian density (Holden, 1976).

In the model considered by Davidsen & Schuster (2002), the rate remains fixed and the threshold process is taken to be ordinary Brownian motion. When the integrated state variable reaches the threshold, an output event is generated and the state variable is reset to some fixed value, as with a conventional integrate-and-reset process. In the case at hand, however, the threshold does not undergo a reset as a result of the generation of the output event. To ensure both a tractable process and finite interevent intervals, the threshold typically has lower and upper reflecting barriers, and these barriers are greater than the state-variable reset values. The persistence of the threshold across interevent intervals renders the process nonrenewal; the power-law exponents associated with $p_\tau(t)$ and $S_N(f)$ therefore need not coincide.

It turns out that the particular form of the integration employed does not qualitatively affect the result; a leaky integrator, for example, yields results similar to those obtained by using the linearly increasing state variable described above. This model generates fractal-based point processes with a rich variety of scaling behavior in both the interevent-interval density $p_\tau(t)$ and the spectrum $S_N(f)$ (Davidsen &

Schuster, 2002). It shows promise in characterizing a number of phenomena in the biological and physical sciences, including action-potential sequences and earthquake occurrences (see Prob. 10.7, however).

Problems

6.1 *Autocorrelation with scaled time* Prove Eq. (6.6) using Eq. (6.1).

6.2 *Stationary increments* Prove Eq. (6.5) using Eq. (6.1).

6.3 *Autocorrelation coefficient* We can define an autocorrelation coefficient of sorts for fractional Brownian motion,

$$\rho(s,t) \equiv \frac{\mathrm{E}[B_H(s)\,B_H(t)]}{\left(\mathrm{E}[B_H^2(s)]\,\mathrm{E}[B_H^2(t)]\right)^{1/2}}\,, \tag{6.28}$$

assuming that neither $s = 0$ nor $t = 0$.

    6.3.1. Find a simplified version of Eq. (6.28), and show that it depends only on the ratio s/t.

    6.3.2. Find a further simplification for the special case $s = -t$ (Mandelbrot, 1982, p. 353). Which values of H make $B_H(t)$ and $B_H(-t)$ independent?

6.4 *Variance of ordinary Brownian motion at unity time* Equation (6.2) provides an expression for $\mathrm{E}[B_H^2(1)]$, the variance of fractional Brownian motion at a time of unity. Show that the resulting expression for ordinary Brownian motion (where $H = \frac{1}{2}$) assumes a value of unity.

6.5 *Generation of ordinary Brownian motion* The midpoint displacement algorithm provides a simple and fast method for generating ordinary Brownian motion, and permits the generation of additional detail (intermediate values) between points already defined. Imagine a realization of ordinary Brownian motion sampled at integer multiples of a sampling time τ_0; we thus have $B(k\tau_0)$ for all integers k. Now we wish to insert intermediate values at times $t = (k + \frac{1}{2})\tau_0$. Let $\mathcal{N}(0,1)$ denote an infinite sequence of Gaussian-distributed random variables with zero mean and unit variance, independent of each other and of the samples $B(k\tau_0)$.

    6.5.1. Given the values $B(k\tau_0)$ and $B[(k+1)\tau_0]$, and a realization of $\mathcal{N}(0,1)$, what value should we insert for $B[(k+\frac{1}{2})\tau_0]$?

    6.5.2. Show that this method does not ignore any other correlations among the inserted values.

    6.5.3. Show that this method fails for general $B_H(k\tau_0)$, remaining valid only for $H = \frac{1}{2}$.

6.6 *Doubly stochastic Poisson process driven by fractal chi-squared rate* Let $\{X_k(t)\}$, $1 \le k \le M$, represent a collection of M independent and identically distributed Gaussian processes with variance $\mathrm{Var}[X]$ and autocorrelation $R_X(t)$. Suppose we set the mean to some large value, such that $\mathrm{E}^2[X]/\mathrm{Var}[X] \gg 1$, and we let one element of the collection $[X_1(t),$ say] serve as a rate for a doubly stochastic

Poisson point process $dN_1(t)$. Suppose further that $dN_1(t)$ has a spectrum that decays as $\sim f^{-\alpha_X}$ with $\frac{1}{2} < \alpha_X < 1$ over some large range of frequencies. Now define $\mu(t) \equiv \sum_{k=1}^{M} \{X_k(t) - \mathrm{E}[X]\}^2$, a fractal chi-squared process, and let this serve as a rate for a separate doubly stochastic Poisson point process $dN_R(t)$.

6.6.1. Show that $dN_R(t)$ has a spectrum that decays as $\sim f^{1-2\alpha_X}$ over an appreciable range of frequencies.

6.6.2. What form does the spectrum take if we do not subtract the mean when generating the rate $\mu(t)$, that is if we consider a fractal noncentral chi-squared process?

6.7 *Spectrum for Poisson process driven by exponentiated-Gaussian process*   Let $X(t)$ denote a dimensionless Gaussian process with mean $\mathrm{E}[X]$, variance $\mathrm{Var}[X]$, and autocorrelation function

$$R_X(t) \approx \mathrm{E}^2[X] + c\ln(t_0/|t|) \tag{6.29}$$

for delay times t in the range $A \ll t \ll B$, with constants $0 < c < 1$ and $t_0 > 0$. Now let $\mu(t) \equiv \exp[X(t)]$ serve as a rate for a Poisson point process. Show that the spectrum of the resulting point process follows a $1/f$-type form for frequencies f in the range $1/B \ll f \ll 1/A$. Also, find the high-frequency asymptote, the fractal exponent α, and an expression for the cutoff frequency f_S.

6.8 *Vesicular exocytosis at the synapse*   Vesicular exocytosis is a mechanism that mediates the passage of cellular signals from one cell to another across the synapse between them (Katz, 1966). Exocytosis also occurs spontaneously, so that neurotransmitter molecules flow across the synapse even in the absence of signaling (Fatt & Katz, 1952), albeit at a substantially reduced rate. Spontaneous exocytosis appears to have its origin in random thermal fluctuations; these cause ion channels to open, which, in turn, admit sufficient calcium into the cell to trigger vesicular exocytosis (Zucker, 1993).

Transition-state theory (Berry, Rice & Ross, 1980) describes the dependence of the expected exocytic rate μ on various parameters of the cells (Hille, 2001), and predicts that it follows the Arrhenius equation,

$$\mu = \mathcal{A}\exp\{-[E_A - \mathsf{q}V]/\mathcal{RT}\}, \tag{6.30}$$

where $\mathcal{A}$ is a rate constant, E_A is a constant activation energy, q is a constant charge associated with the transition, $\mathcal{R}$ is the thermodynamic gas constant, $\mathcal{T}$ is the absolute temperature, and V is the membrane voltage of the presynaptic cell.

6.8.1. What point process would be a suitable candidate for describing the sequence of exocytic events if the membrane voltage V is fixed?

6.8.2. How would the collection of processes associated with multiple cells be described if we assume that V is constant for each cell, but varies across cells?

6.8.3. In actuality, the membrane resting voltage V does not remain fixed, but rather exhibits a Gaussian amplitude distribution with fractal ($1/f$-type) fluctuations (Verveen & Derksen, 1968; Holden, 1976; Stern et al., 1997). This suggests that the membrane voltage may be described by a fractal Gaussian process. Show how

this leads to the fractal lognormal-noise-driven Poisson process as a model for the spontaneous vesicular exocytosis process in real preparations (Lowen et al., 1997a,b). We have already demonstrated that neither a fractal point process nor a multifractal point process provides a good description for these data (see Prob. 5.5.3 and Fig. 5.11).